Int. J. Heat Mass Transfer. Vol. 36, No. 1, pp. 35–47, 1993
Printed in Great Britain

0017-9310/93 $5.00 + 0.00


# Natural convection in a heated annulus

B. B. ROGERS and L. S. YAO
Department of Mechanical and Aerospace Engineering, Arizona State University, Tempe, AZ 85287, U.S.A.

(*Received* 12 *February* 1992 *and in final form* 7 *April* 1992)

**Abstract**—Natural convection in a heated vertical concentric annulus is studied. A constant heat-flux is applied to the inner cylinder and the outer cylinder is insulated. Under these conditions, the mean temperature of the fluid increases linearly while, at the same time, heat diffuses from the heated surface into the fluid, resulting in a temperature distribution on the cross-section. Subtracting this steadily increasing temperature from the total temperature results in a steady temperature stratification on the cross-section which drives fluid motion. The mathematical form of the scaled problem is shown to be identical to that of a fluid in an annulus with uniformly distributed heat sources, with the inner cylinder maintained at constant temperature and the outer cylinder insulated. At low heat addition rates, the fluid motion is steady and parallel, and heat is transferred by conduction between the fluid layers. As the rate of heating increases, the flow becomes unstable and recirculating eddies appear, which transfer heat by convection. The onset of convection is determined by linear-instability analysis of the basic-state. The results demonstrate that when the Prandtl number is small, the dominant instability obtained energy primarily from shear production. On the other hand, when the Prandtl number is large, an instability that obtains kinetic energy from buoyant production is pre-eminent. Weakly nonlinear instability theory is used to analyze finite-amplitude effects. The results show that both types of linear instabilities are supercritical.

## 1. INTRODUCTION

INSTABILITY of natural convection in a tall vertical channel or annulus has been extensively studied due to its relevance to practical applications, as well as being a model problem for thermally driven flow instabilities [1–7]. The flow can be shown to depend on the Grashof number ($Gr$), the Prandtl number ($Pr$) and the geometry of the enclosure. In a tall vertical slot, when the flow is assumed to be parallel, the resulting velocity profile is cubic, with the fluid near the warmer wall moving upward and that near the cooler wall moving down [1]. In a parallel flow, heat is transferred across the duct solely by conduction between the fluid layers, and the flow is said to be in the conduction regime. The experimental results of Eckert and Carlson [2] and Elder [3, 4] confirmed the existence of the conduction regime when $Gr$ is small. As $Gr$ increases, however, the flow becomes unstable, first resulting in multicellular secondary flow patterns, and, as $Gr$ increases further, turbulence. The stability of the conduction regime of natural convection has also been investigated [6–9]. The findings demonstrate that for low $Pr$ fluids, the dominant instability is insensitive to changes in $Pr$ and is due to an unstable velocity distribution induced by thermal effects. Therefore, this is a *thermal-shear* instability, which obtains kinetic energy primarily by shear production. At large $Pr$, however, another instability becomes pre-eminent. This is called the *thermal-buoyant* instability since it obtains kinetic energy primarily from the buoyant force. In all of these studies, the wall temperatures are held constant, and the temperature difference between each wall induces a thermal stratification that drives fluid motion. The instability occurs when the temperature difference becomes larger than a threshold value. This corresponds to the critical Grashof number. However, the $Pr$ effects on flow instabilities have never been systematically studied; consequently, our understanding of the $Pr$ effects is incomplete.

There is a class of natural convection problems of practical importance which have not been studied previously, where the temperature of the fluid may continuously increase due to a constant heat flux condition on one of the surfaces. For example, a key problem in the storage of nuclear wastes is the determination of the insulating effect of the annular air space surrounding a cylindrical nuclear waste canister embedded in a geologic repository. In this situation, heat will be transferred from the canister, through the insulating air space and into the surrounding rock. Heat may be transferred through the air space by conduction between the fluid layers, and by convection. If the buoyancy induced motion of the air is laminar and parallel, heat will be transferred solely by conduction between the fluid layers, and the thermal resistance of the air gap will be relatively large. However, if the motion of the air becomes unsteady and recirculating eddies appear, heat will also be transferred through the air by convection due to the transverse mixing of the fluid. In this case, the thermal resistance of the air gap will be much smaller than in the case of pure conduction and the equilibrium temperature of the canister will be correspondingly lower. It has been estimated that the properties of the air gap can affect the final equilibrium temperature of the canister by as much as 350°F (177°C) [10]. This

## NOMENCLATURE

| | |
|---|---|
| $A$ | small amplitude of disturbance wave |
| $a_1$ | first Landau coefficient |
| $B$ | order-one amplitude function, $(c_i)^{1/2}A$ |
| $c$ | complex disturbance wavespeed, $c_r+ic_i$ |
| $g$ | gravitational acceleration |
| $h$ | convective heat transfer coefficient |
| $Gr$ | Grashof number, $W_s(r_o-r_i)/\nu$ |
| $k$ | thermal conductivity |
| $k$ | rate of increase of fluid temperature |
| $K$ | curvature parameter for the annulus, $r_i/(r_o-r_i)$ |
| $Nu$ | Nusselt number |
| $n$ | azimuthal wavenumber |
| $p, P, \hat{p}$ | pressure |
| $Pr$ | Prandtl number, $\nu/\hat{\alpha}$ |
| $r_i, r_o$ | inner and outer radii of concentric cylinders |
| $T_w$ | temperature of inner wall of annulus |
| $T_0$ | initial inner wall temperature |
| $t$ | time |
| $u, \hat{u}$ | radial velocity |
| $v, \hat{v}$ | azimuthal velocity |
| $w, W, \hat{w}$ | axial velocity |
| $W_s$ | velocity scale, $g\beta k(r_o-r_i)^4/\nu^2$ |
| $z$ | axial coordinate. |

Greek symbols

| | |
|---|---|
| $\alpha$ | axial wavenumber |
| $\hat{\alpha}$ | thermal diffusivity |
| $\beta$ | thermal expansion coefficient |
| $\Delta$ | distance from neutral curve, $\lvert Gr-Gr_c\rvert$ |
| $\eta$ | radial coordinate |
| $\theta, \Theta, \hat{\theta}$ | dimensionless temperature |
| $\nu$ | kinematic viscosity |
| $\rho$ | density |
| $\tau$ | slow time scale |
| $\phi$ | azimuthal coordinate. |

temperature is critical because it is the primary factor which determines the life span of the metal containers. To determine if heat will be transferred through the air gap by conduction or convection, the stability of the parallel motion must be investigated. As will be demonstrated, the criterion for flow instability will depend on the rate of heat addition to the air. Therefore, due to increased thermal resistance in the surrounding air gap, it is possible that a canister with a low rate of heat production, so that flow instability is not induced, could reach a higher equilibrium temperature than a canister with a heat flux high enough to induce instability. In this paper, this problem will be studied by considering the buoyancy-driven flow of a fluid in a vertical annulus with a constant heat-flux applied to the inner cylinder and the outer cylinder insulated. This models the early state of the waste storage system. The model may also be used to study the abnormal core condition of a nuclear reactor in a reflood phase. In this situation, the fuel rods form an array of cylindrical heating elements in the reactor vessel and the behavior of the flow near each individual fuel rod may be approximated as an annular region with the inner cylinder heated and the outer cylinder insulated.

It is worthwhile to note that the problem studied in this paper is a limit of mixed-convection with zero mean flow. The linear-instability analysis of mixed-convection in a vertical annulus with the inner cylinder heated and the outer cylinder insulated [11] found that the thermal instability may be a thermal-shear type, a thermal-buoyant type, or a Rayleigh–Taylor type, depending on the value of $Pr$ and the vertical density stratification of the fluid. When the vertical temperature gradient is negative, a Rayleigh–Taylor type instability is possible since the vertical density stratification is unstable. In the stably stratified case, the Rayleigh–Taylor mode is not present, and the thermal instability will be either a thermal-shear mode at small $Pr$, or a thermal-buoyant mode at large $Pr$. The results showed that all the thermally induced instabilities exhibited very little $Re$ dependence except at $Re$ below 200, in qualitative agreement with the experimental observations of Maitra and Subba Raju [12].

As will be discussed in Section 2, in the natural convection problem with a constant heat-flux condition on the inner cylinder, the mean system temperature will increase linearly with time. Simultaneously, the heat will diffuse into the fluid from the heated cylinder resulting in a temperature distribution on the cross-section. The temperature scale is then determined by considering the ratio of the two time scales associated with the wall heating rate and the diffusivity of the fluid. In this case, because of the finite geometry of the annulus, the temperature reaches a quasi-equilibrium in which the temperature of the fluid increases uniformly everywhere on the cross-section. By subtracting this continuously increasing temperature from the total temperature, a steady fluid temperature distribution is obtained, which induces fluid motion. The result of this scaling is that the rate of increase of fluid temperature shows up in the dimensionless energy equation as a constant source term. Consequently, the mathematical form of the scaled problem in this case is identical to that of a fluid in an annulus with the inner cylinder maintained at a constant temperature and the outer cylinder insulated, with uniformly distributed heat sources in the fluid. Therefore, a comparison of data

from experiments of the current problem and those of uniform internal energy generation will be related one-to-one.

The dimensionless steady basic-state is a function of the radial coordinate only, and is independent of $Gr$ and $Pr$, where $Gr$ is the Grashof number defined in terms of the rate of increase of the fluid temperature. The analysis of the linear and nonlinear instability of the basic-state is described in Sections 2.3 and 2.4. Results of the instability analyses presented in Section 3.1 demonstrate that two types of thermally induced instabilities are present. The first is pre-eminent at small $Pr$, and is the thermal-shear instability. The second dominates at large $Pr$, and is the thermal-buoyant instability. The weakly nonlinear calculations indicate that both of the instabilities are supercritical under all conditions. With both instabilities, it is found that the first azimuthal mode is the most unstable when the curvature of the annulus is large, and the least stable mode becomes axisymmetric as the curvature decreases. The thermal-shear instability is insensitive to changes in $Pr$. With the thermal-buoyant mode, however, a significant $Pr$ dependence appears, and $Gr_c$ decreases as $Pr$ increases. The increase in the mean Nusselt number due to the first transition is calculated using the results of the finite-amplitude analysis, and the results show that flow instability leads to a noticeable increase in the value of $Nu$ due to transverse mixing of the fluid. In Section 4, the balances of disturbance kinetic energy and thermal variance are considered. The results demonstrate the means by which the potential energy associated with the temperature fluctuations and the kinetic energy of the velocity fluctuations are exchanged.

## 2. ANALYSIS

### 2.1. *Formulation*

The problem considered in this paper is that of the buoyancy-driven motion of a viscous fluid enclosed in a tall vertical cylindrical annulus as illustrated in Fig. 1. A uniform heat flux is applied at the inner cylinder and the outer cylinder is insulated, and, as a consequence, the fluid mean temperature is increasing linearly with time. This temperature increase is given by

$$k = Pr\frac{dT_w}{d\hat{t}} \tag{1}$$

where $T_w$ is the temperature of the inner wall, $\hat{t}$ the dimensional time and $Pr$ the Prandtl number. The inclusion of the factor of $Pr$ in this definition results in a more convenient form for the dimensionless governing equations, as will be explained below.

As the inner cylinder is heated, the heat will diffuse into the fluid, creating a temperature distribution on the cross-section. Therefore, the temperature difference between the cylinder wall and the fluid will be proportional to the ratio of time scales associated with

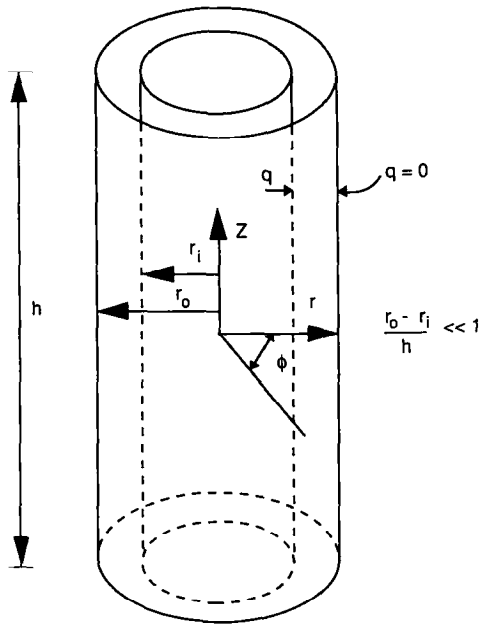


FIG. 1. Geometry and coordinates.

the fluid heating and the diffusion process. However, when the heat-flux is first initiated, the temperature distribution will be concentrated near the inner wall since the heat will require a finite period of time to conduct into the fluid. Since the geometry of the annulus is finite, a quasi-steady temperature distribution will eventually result in which the fluid temperature is increasing uniformly on the cross-section. The quasi-steady distribution will be established when the time is much larger than the conduction time, given by $\hat{t}_c = (r_o - r_i)^2/\hat{\alpha}$, where $\hat{\alpha}$ is the fluid thermal diffusivity, and $r_o$ and $r_i$ are the outer and inner radii of the concentric annulus. A momentum diffusion time, equal to the conduction time divided by $Pr$, may also be defined. The temperature difference between the wall and the fluid will therefore be as follows:

$$T_w - T \sim \frac{k(r_o - r_i)^2}{\nu}$$

where $\nu$ is the kinematic viscosity. This leads to the following definition of a dimensionless temperature:

$$\theta = \frac{(T_w - T)\nu}{k(r_o - r_i)^2}. \tag{2}$$

The *mean* value of $\theta$ will be independent of time when the time is large compared with the conduction time since both $T_w$ and $T$ are increasing at a rate proportional to $k$. However, at all times $\theta$ may fluctuate about its mean value due to recirculating eddies that result from hydrodynamic instability.

The thermal velocity scale for the problem is obtained by balancing the viscous shear force and the buoyant force in the vertical momentum equation. The result is

$$W_s \sim \frac{g\beta\Delta T(r_o - r_i)^2}{\nu}$$

where $g$ is the acceleration of gravity and $\beta$ is the thermal expansion coefficient. In this problem, however

$$\Delta T = T_w - T.$$

Therefore

$$W_s = \frac{g\beta k(r_o - r_i)^4}{\nu^2}. \tag{3}$$

The governing equations are the Navier–Stokes equations with the Boussinesq approximation in cylindrical coordinates. Using the scales defined above for velocity and temperature, in dimensionless form they become

$$\frac{\partial u}{\partial \eta} + \frac{u}{\eta + K} + \frac{1}{\eta + K}\frac{\partial v}{\partial \phi} + \frac{\partial w}{\partial z} = 0 \tag{4a}$$

$$\frac{\partial u}{\partial t} + u\frac{\partial u}{\partial \eta} + \frac{v}{\eta + K}\frac{\partial u}{\partial \phi} + w\frac{\partial u}{\partial z} - \frac{v^2}{\eta + K} = -\frac{\partial p}{\partial \eta} + \frac{1}{Gr}\left(D^2 u - \frac{1}{(\eta + K)^2}\left(2\frac{\partial v}{\partial \phi} + u\right)\right) \tag{4b}$$

$$\frac{\partial v}{\partial t} + u\frac{\partial v}{\partial \eta} + \frac{v}{\eta + K}\frac{\partial v}{\partial \phi} + w\frac{\partial v}{\partial z} + \frac{uv}{\eta + K} = -\frac{1}{\eta + K}\frac{\partial p}{\partial \phi} + \frac{1}{Gr}\left(D^2 v + \frac{1}{(\eta + K)^2}\left(2\frac{\partial u}{\partial \phi} - v\right)\right) \tag{4c}$$

$$\frac{\partial w}{\partial t} + u\frac{\partial w}{\partial \eta} + \frac{v}{\eta + K}\frac{\partial w}{\partial \phi} + w\frac{\partial w}{\partial z} = -\frac{\partial p}{\partial z} + \frac{1}{Gr}(D^2 w - \theta) \tag{4d}$$

$$\frac{\partial \theta}{\partial t} + u\frac{\partial \theta}{\partial \eta} + \frac{v}{\eta + K}\frac{\partial \theta}{\partial \phi} + w\frac{\partial \theta}{\partial z} = \frac{1}{Gr\,Pr}(D^2\theta + 1) \tag{4e}$$

where

$$D^2 = \frac{\partial^2}{\partial \eta^2} + \frac{1}{\eta + K}\frac{\partial}{\partial \eta} + \frac{1}{(\eta + K)^2}\frac{\partial^2}{\partial \phi^2} + \frac{\partial^2}{\partial z^2}.$$

The above equations have been made dimensionless by scaling the lengths with the annular gap width, $r_o - r_i$, time by $(r_o - r_i)/W_s$, velocities by $W_s$, and pressure by $\rho W_s^2$ where $\rho$ is the density. The dimensionless radial coordinate is $\eta = (r - r_i)/(r_o - r_i)$, and a curvature parameter for the annulus has been defined as $K = r_i/(r_o - r_i)$. The parameters in the problem are the Grashof number, $Gr = W_s(r_o - r_i)/\nu$, and the Prandtl number, $Pr = \nu/\hat{\alpha}$. Therefore, in this problem $Gr$ is a measure of the rate of heat addition to the fluid.

Investigation of the energy equation (4e) shows that the time dependence of the temperature has been separated into two parts. The first accounts for temperature fluctuations about the mean and is given by $\partial\theta/\partial t$. The second term represents the steady linear increase in fluid temperature and, after nondimensionalization, is given by $1/(Gr\,Pr)$. The inclusion of the factor of $Pr$ in the definition of $k$ given in equation (1) makes it possible to group this term with the conduction terms, as has been done in equation (4e), resulting in a basic-state that does not depend on $Pr$.

### 2.2. *Basic-state*

The basic-state of the flow is a steady, fully developed parallel flow. If we apply these conditions to equations (4a)–(4e), the basic-state will be a function of the radial coordinate only, and the equations simplify to the following

$$\frac{d^2 W_0}{d\eta^2} + \frac{1}{\eta + K}\frac{dW_0}{d\eta} - \Theta_0 = Gr\frac{dP_0}{dz} \tag{5a}$$

$$\frac{d^2\Theta_0}{d\eta^2} + \frac{1}{\eta + K}\frac{d\Theta_0}{d\eta} = -1 \tag{5b}$$

where $W_0$ and $\Theta_0$ are the basic-state velocity and temperature, respectively. The boundary conditions on the basic-state are

$$W_0(0) = W_0(1) = \Theta_0(0) = \Theta_0'(1) = 0. \tag{5c}$$

The term $Gr(dP_0/dz)$ is determined by the requirement of global mass conservation

$$\int_0^1 W_0(\eta + K)\,d\eta = 0. \tag{6}$$

Consequently, the basic-state is independent of $Gr$ and $Pr$, but will depend on the value of $K$. The effect of scaling the temperature by the rate of increase of the mean temperature may be clarified by investigation of the energy equation for the basic-state, equation (5b). The steady temperature increase shows up in this equation as the nonhomogeneous term, $-1$. Therefore, it appears as a uniform source term which modifies the dimensionless radial temperature distribution, $\Theta_0$.

It is possible to solve the basic-state equations analytically by the use of Bessel functions. However, the solution is tedious and it is found to be more convenient to solve the equations numerically using a spectral/collocation technique, which was later used as part of the linear-instability analysis. Basic-state velocity and temperature profiles for $K = 0.6$ and 10 are shown in Fig. 2. As these results show, the velocity profile for $K = 10$ is almost symmetric about $\eta = 0.5$, while the profile for $K = 0.6$ is asymmetric. This is because $K = 10$ corresponds to an annulus with a narrow gap, approaching a two-dimensional slot, while $K = 0.6$ represents an annulus with a much more pronounced curvature effect. Both of these velocity profiles contain inflection points, which suggests a potential for inviscid instability.

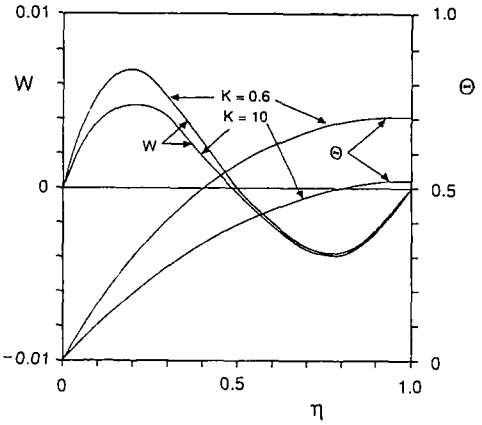


FIG. 2. Basic-state velocity and temperature profiles.

2.3. *Linear-instability*

Linear-instability is studied by subtracting the basic-state from the governing equations, and neglecting the small nonlinear terms. Although this is a transient heating problem, a normal mode form may be assumed for the disturbance because the temperature has been scaled by the rate of temperature increase. Therefore, the dependent variables are written as follows:

$$u(\eta,\phi,z,t) = \hat{u}(\eta)\,e^{i\alpha(z-ct)+in\phi} \tag{7a}$$

$$v(\eta,\phi,z,t) = \hat{v}(\eta)\,e^{i\alpha(z-ct)+in\phi} \tag{7b}$$

$$w(\eta,\phi,z,t) = W_0(\eta)+\hat{w}(\eta)\,e^{i\alpha(z-ct)+in\phi} \tag{7c}$$

$$\theta(\eta,\phi,z,t) = \Theta_0(\eta)+\hat{\theta}(\eta)\,e^{i\alpha(z-ct)+in\phi} \tag{7d}$$

where $\alpha$ is the axial wavenumber, $n$ the integer azimuthal wavenumber, $c$ the complex disturbance wavespeed and '$\hat{}$' denotes the small disturbance component of the dependent variable. The result is a set of linear ordinary differential equations given by

$$\hat{u}'+\frac{\hat{u}}{\eta+K}+\frac{in\hat{v}}{\eta+K}+i\alpha\hat{w}=0 \tag{8a}$$

$$i\alpha\,Gr(W_0-c)\hat{u}+Gr\,\hat{p}'-\hat{u}''-\frac{\hat{u}'}{\eta+K}+\frac{\hat{u}}{(\eta+K)^2}+\frac{n^2\hat{u}}{(\eta+K)^2}+\alpha^2\hat{u}+\frac{2in\hat{v}}{(\eta+K)^2}=0 \tag{8b}$$

$$i\alpha\,Gr(W_0-c)\hat{v}+\frac{in\,Gr\,\hat{p}}{\eta+K}-\hat{v}''-\frac{\hat{v}'}{\eta+K}+\frac{\hat{v}}{(\eta+K)^2}+\frac{n^2\hat{v}}{(\eta+K)^2}+\alpha^2\hat{v}-\frac{2in\hat{u}}{(\eta+K)^2}=0 \tag{8c}$$

$$i\alpha\,Gr(W_0-c)\hat{w}+Gr\,\hat{u}W_0'+i\alpha\,Gr\,\hat{p}-\hat{w}''-\frac{\hat{w}'}{\eta+K}+\frac{n^2\hat{w}}{(\eta+K)^2}+\alpha^2\hat{w}+\hat{\theta}=0 \tag{8d}$$

$$i\alpha\,Gr\,Pr(W_0-c)\hat{\theta}+Gr\,Pr\,\hat{u}\Theta_0'-\hat{\theta}''-\frac{\hat{\theta}'}{\eta+K}+\frac{n^2\hat{\theta}}{(\eta+K)^2}+\alpha^2\hat{\theta}=0 \tag{8e}$$

where the prime denotes differentiation with respect to $\eta$. These equations form an eigenvalue problem for the complex disturbance wavespeed, $c$, with the disturbance being unstable for $c_i$ greater than zero.

The equations for the basic-state and disturbance were discretized using a spectral Chebyshev collocation technique and the stability boundary was determined by a numerical search of the parameter space to determine the locus of points where $c_i = 0$. Details of the numerical procedure may be found in ref. [5]. For particular values of the Prandtl number and curvature parameter, the point on the neutral curve at which the flow first becomes unstable defines the minimum critical Grashof number, $Gr_c$.

2.4. *Finite-amplitude instability*

Linear-instability theory determines the point at which an infinitesimal disturbance becomes unstable, and predicts unbounded exponential growth of the disturbance. As the disturbance grows to finite size, however, nonlinear effects modify the growth rate predicted by linear theory. To study these effects, the weakly nonlinear instability theory developed in ref. [13] is applied to this problem.

To study finite-amplitude instability using a weakly nonlinear theory, the dependent variables are first separated into Fourier components of a disturbance wave predicted by linear-instability theory. The equations governing the harmonic components are then solved using a perturbation expansion. There are different versions of weakly nonlinear theories that differ in the choice of a small parameter. Stuart [14] used the imaginary portion of the eigenvalue, $c_i$, which is proportional to the disturbance amplification rate, to order the harmonic equations. Watson [15] used the amplitude of the disturbance, $A$. Stewartson and Stuart [16] used the distance from the neutral curve, $\Delta = Re - Re_c$. On the other hand, as was demonstrated in ref. [13], definite physical relationships exist between these parameters. The theories of refs. [14, 16] consider these relations in a consistent manner in the ordering of terms in the perturbation expansions. As a consequence, both theories involve expansions in terms of a single small parameter, $c_i$ or $\Delta$, and are equally valid for both subcritical and supercritical flows. The theories are asymptotically identical in problems for which a neutral curve exists. (However, the theory of ref. [14] may also be used in problems without a neutral curve as long as the magnitude of $c_i$ is small enough.) In nonisothermal flow, however, it has been observed that the expansion in $\Delta$ breaks down quickly because of the presence of branch-point type singularities in the perturbation series that links $c_i$ and $\Delta$ [13], and the expansion in terms of $c_i$ is more convenient. The expansion of ref. [13] represents a small modification to that of ref. [14], in that the terms involving the difference between the basic-state velocity and the complex disturbance wavespeed, $(W_0-c)$, are considered to be of the order of one. This is because the finite-amplitude instability dis-

turbance is expressed as a perturbation on the state of a finite amplification rate, $c_i$. Consequently, the Landau constants can be uniquely determined without any specially designed normalization scheme.

To explain the differences between the theories, consider the evolution of the amplitude of a supercritical instability with increasing $Gr$, as shown in Fig. 3. In Fig. 3, point C corresponds to the neutral point of linear-instability, with $Gr = Gr_c$, and points D and E are at a supercritical value of $Gr$, $Gr > Gr_c$. In the theory of ref. [16], the expansion is anchored at the neutral curve, which is point C. All of the relevant functions are calculated at this point, and points C and D are linked by a perturbation expansion in $\Delta$. In ref. [13], on the other hand, the expansion is anchored at point D, and the relevant functions are calculated at this point. An advantage in this approach is that the expansion in $\Delta$ between points C and D is eliminated. This also explains why the term $(W_0 - c)$ is considered to be of the order of one in ref. [13], since $c_i$ is non-zero at point D.

In this problem, the Fourier expansion of, for example, the axial velocity is written as follows:

$$w(\eta, \phi, z, t) = W(\eta, \tau)E^0 + w_1(\eta, \tau)E^1 + w_2(\eta, \tau)E^2 + \cdots + \text{c.c.} \quad (9)$$

where $E = \exp(i\alpha(z - c_r t) + in\phi)$, $\alpha$ the axial wavenumber corresponding to $Gr_c$, and $c_r$ the wavespeed of the most unstable disturbance, given by the real portion of the eigenvalue from linear theory. In this problem, we will obtain only the lowest order correction to the exponential growth predicted by linear theory, and inclusion of $E^3$ and higher harmonics is not necessary.

The functions for the harmonic components are further decomposed by expanding in terms of the small parameter. Using the method of multiple scales with $(t, \tau = c_i t)$ results in

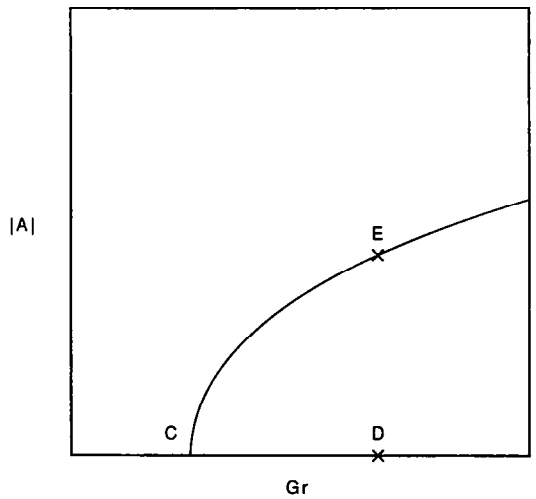


FIG. 3. Illustration of supercritical bifurcation.

$$\frac{\partial}{\partial t} = \frac{\partial}{\partial t} + c_i \frac{\partial}{\partial \tau}. \quad (10)$$

The following expansion of the $E^1$ wave is consistent

$$w_1(\eta, \tau) = c_i^{1/2} B(\tau) w_{10}(\eta) + c_i^{3/2} B|B|^2 w_{11}(\eta) + O(c_i^{5/2}) \quad (11)$$

where $B$ is an order-one amplitude function. The physical amplitude of the $w_{10}$ functions is therefore $A = (c_i)^{1/2} B$. The expansion for the $E^1$ wave given by equation (12) leads to the following forms for the $E^0$ and $E^2$ waves:

$$W(\eta, \tau) = W_0(\eta) + c_i |B(\tau)|^2 W_1(\eta) + O(c_i^2) \quad (12)$$

$$w_2(\eta, \tau) = c_i (B(\tau))^2 w_{20}(\eta) + O(c_i^2). \quad (13)$$

Terms of the order of $(c_i)^2$ and smaller are not necessary in the present analysis. Expansions of the other dependent variables corresponding to equations (9) through to (13) are given by similar expressions. The system of harmonic equations obtained by substituting equation (9) through equation (13) into the governing equations may be solved sequentially in increasing powers of $c_i$. At the order of $(c_i)^0$ the only non-zero contribution is from the $E^0$ equations, which become those of the basic-state. Therefore, the functions $W_0$ and $\Theta_0$ are given by basic-state velocity and temperature distributions, respectively. At the order of $(c_i)^{1/2}$, the $E^1$ equations become those of linear-instability, and the other harmonic components are zero. Consequently, the functions $u_{10}$, $v_{10}$, $w_{10}$ and $\theta_{10}$ are given by the eigenvectors of linear theory at the particular values of $Gr$, $\alpha$ and $n$ being considered. At the order of $c_i$, the equations for the $E^0$ and $E^2$ waves produce nonhomogeneous equations for the mean-flow distortion functions, $W_1$ and $\Theta_1$, and for the harmonic functions, $u_{20}$, $v_{20}$, $w_{20}$ and $\theta_{20}$. The nonhomogeneous terms in these equations involve only the functions $u_{10}$, $v_{10}$, $w_{10}$ and $\theta_{10}$, which are known from lower-order analysis. Therefore, these equations may be easily solved, since the amplitude function factors out on each side of the equations and may be canceled. At the order of $(c_i)^{3/2}$, the $E^1$ equations become nonhomogeneous equations with the left-hand sides consisting of the linear-instability operators operating on the functions $u_{11}$, $v_{11}$, $w_{11}$ and $\theta_{11}$, and the right-hand sides consisting of terms proportional to $dB/d\tau$, $B$ and $B|B|^2$. The coefficients of the terms on the right-hand sides consist of the functions determined from the analysis at lower-orders. Since the homogeneous forms of the equations are exactly those of linear-instability theory, the integrability condition requires that the right-hand sides be orthogonal to the functions satisfying the homogeneous adjoint problem. This condition leads to a Landau equation

$$\frac{dB}{d\tau} = \alpha B + a_1 B|B|^2. \quad (14)$$

The constant $a_1$ is the first Landau constant, and

is obtained through application of the integrability condition. Equation (14) represents a modification to the exponential growth or decay of a disturbance predicted by linear theory. If the real part of $a_1$ is negative, a supercritical equilibrium amplitude is predicted as $|A|^2 = c_i|B|^2 = -\alpha c_i/(a_1)_r$, where the subscript r denotes the real part. In the case of $(a_1)_r$ positive, a subcritical instability is predicted with a threshold amplitude of $|A|^2 = |\alpha c_i/(a_1)_r|$.

In addition to the disturbance amplitude, the weakly nonlinear theory predicts the following order $c_i$ modulation to the wavespeed due to the disturbance growth [14]

$$c_r' = c_r + c_i \frac{(a_1)_i}{(a_1)_r} \tag{15}$$

where $c_r$ is the wavespeed predicted by linear theory, and $(a_1)_i$ is the imaginary portion of the first Landau constant.

It is worthwhile to note that the Landau constants obtained by amplitude expansions [15, 17–19], which have been extensively developed because of ease of inclusion of higher-order terms, will not be the same as those obtained by the theory of ref. [13]. This is because amplitude expansions ignore the ordering between $c_i$ and $A$, and some higher-order terms, proportional to $c_i$, are prematurely considered in the lower-order equations. This results in two serious problems with these techniques. The first is that the Landau constants are not determined uniquely, unless $c_i = 0$. The second is that the mean-flow equations possess resonant solutions in the subcritical region [20]. The amplitude expansion theories have been unsuccessful in overcoming these problems. On the other hand, in the equilibrium amplitude method [17], $d|A|^2/dt$ is set equal to zero at the outset, and only equilibrium states are sought. With this procedure, the analysis is considerably simplified, and the problems of nonuniqueness of the Landau constants and mean-flow resonance are eliminated in the lowest-order perturbation equations. In fact, to the lowest order, the method of ref. [17] produces the same result as the consistent theory of ref. [13]. However, if higher-order terms are considered the results will differ since the terms proportional to $c_i$ have been identically set to zero in the equilibrium amplitude approach rather than deferred to higher order, as they are in ref. [13], and the problem of nonuniqueness of Landau constants persists at higher orders.

## 3. RESULTS

### 3.1. *Results of instability calculations*

The parameters in this problem are $Gr$, $Pr$ and $K$. At fixed $Pr$ and $K$, the flow becomes unstable as $Gr$ increases, and a complete linear-instability map is obtained by considering the effect of both $Pr$ and $K$ on $Gr_c$. In this paper, the effect of $Pr$ on $Gr_c$ is studied at two values of $K$: $K = 0.6$ and 10. In addition, the effect of $K$ on $Gr_c$ is analyzed at fixed Prandtl numbers of 0.01 and 10. As will be discussed in more detail below, these choices of $Pr$ and $K$ provide a complete picture of the instabilities present in this problem. It is worthwhile to point out that it is known from kinetic theory that ideal gases will have Prandtl numbers greater than 0.4, while most common liquids have Prandtl numbers greater than 1. The exceptions are liquid metals, whose Prandtl numbers are less than 0.1. Consequently, no common fluids will have Prandtl numbers in the intermediate range. However, data are presented for a continuous range of $Pr$ to clarify the results of the instability calculations.

Figure 4 is a plot of $Gr_c$ vs $Pr$ for $K = 0.6$ and 10. The results in Fig. 4 clearly indicate that two types of instabilities are present. At small values of $Pr$ the dominant instability is insensitive to changes in $Pr$ in both geometries. On the other hand, at larger values of $Pr$, another instability appears which is strongly dependent on $Pr$, with $Gr_c$ decreasing with increasing $Pr$. As will be proven in Section 4, the low $Pr$ instability is hydrodynamic in origin, resulting from an unstable velocity profile induced by thermal effects, and is therefore a thermal-shear instability, since it obtains most of its kinetic energy through shear production. The large $Pr$ instability is fundamentally different from the thermal-shear instability since it obtains most of its kinetic energy from buoyant production, and is called the thermal-buoyant instability.

At $K = 0.6$, the thermal-shear instability is dominant for $Pr$ less than 0.4. The value of $Gr_c$ initially decreases rapidly as $Pr$ increases for the thermal-buoyant mode, but at large values of $Pr$, $Gr_c$ reaches a constant value of about $Gr_c = 700$. Therefore, in this geometry, if the fluid is a liquid metal, the most unstable linear disturbance will be the thermal-shear mode, while other common fluids will become unstable to the thermal-buoyant mode. On the other hand, with $K = 10$, the thermal-buoyant mode is not pre-eminent until $Pr$ is larger than 7. This shows that as $K$ increases, resulting in a smaller curvature effect, the minimum Prandtl number for which the thermal-buoyant instability is dominant increases. It is worthwhile to point out that $Pr = 7$ is within the range of variation of $Pr$ for many common fluids. For example, with water $Pr$ is greater than 7 for temperatures below 18°C, and less for higher temperatures. Consequently, as the water temperature increases, the most linearly unstable mode changes from the thermal-buoyant mode at low temperatures to the thermal-shear mode at higher temperatures. Since the critical value of $Gr$ is less for the thermal-buoyant mode than it is for the thermal-shear mode, a linearly unstable flow of water at $Gr = 10\,000$, for example, will be stabilized due to fluid property variations as the water temperature increases.

Figure 5 is a plot of $Gr_c$ vs $K$ at $Pr = 0.01$ and 10, the smaller Prandtl number being representative of the thermal-shear instability and the larger of the thermal-buoyant instability. For the thermal-shear instability,

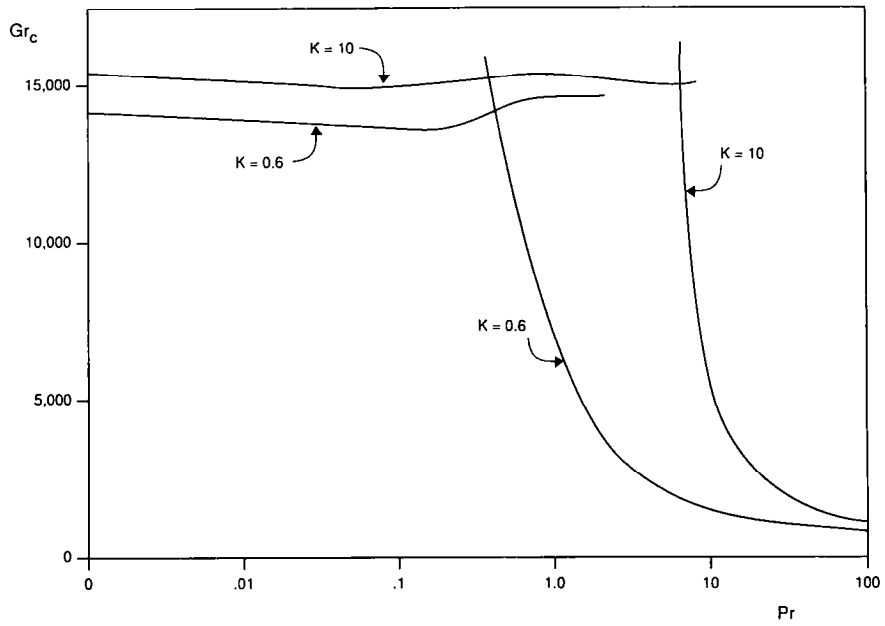


FIG. 4. Critical Grashof number vs Prandtl number for $K = 0.6$ and 10.

$n = 1$ is the dominant azimuthal mode for $K$ less than 0.7, with $n = 0$ the most unstable mode for $K$ larger than this value. $Gr_c$ is smallest at small values of $K$ and increases with increasing $K$, approaching a value of $Gr_c = 15\,200$ at large $K$. With the thermal-buoyant instability, $n = 1$ is the dominant mode for values of $K$ less than 0.9. Similar to the thermal-shear mode, $Gr_c$ increases with increasing $K$, and at large values of $K$ approaches a constant value of $Gr_c = 6100$. In this problem, in the limit of a two-dimensional slot Squire's theorem may be proven. Therefore, the fact that $n = 0$ becomes the dominant mode as $K$ increases is expected.

The first Landau constant has been calculated at points on the curves shown in Figs. 4 and 5, and the results of the calculations at four points are given in Table 1. As the results show, these instabilities are all superficial. In fact, in a search of the entire ($Pr$, $K$, $n$, $\alpha$) space at the critical values of $Gr$, revealed no subcritical instabilities. Therefore, in all cases, at low heating rates, the fluid motion will be steady and parallel, and will remain in this condition until the flow becomes linearly unstable, since there are no subcritically unstable states. In this condition, heat will be transferred across the duct solely by conduction. As the rate of heating increases, the flow will undergo a transition to multicellular convection, which will begin when the critical Grashof number for linear-instability is exceeded. In the neighborhood of $Gr_c$, an unstable disturbance will grow until it reaches an equilibrium amplitude equal to $(-\alpha c_i/(a_1)_r)^{1/2}$.

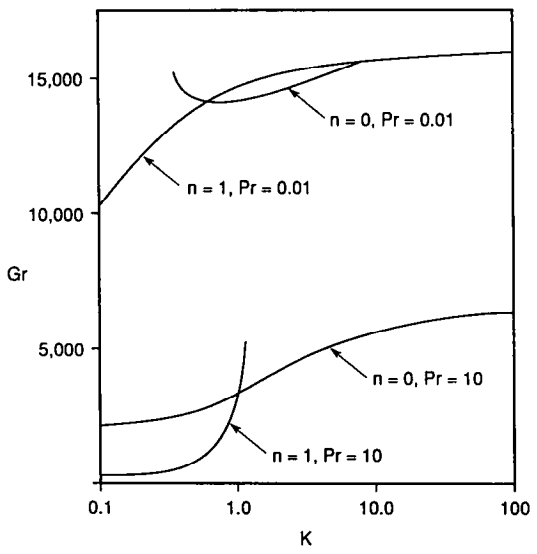


FIG. 5. Critical Grashof number vs $K$ for $Pr = 0.01$ and 10.

The results in Figs. 4 and 5 have demonstrated that there are two types of instabilities for this flow, and both instabilities become linearly unstable to the first azimuthal mode at small $K$, and the axisymmetric mode at large $K$. For all values of $Pr$, at $K = 0.6$, the most unstable azimuthal mode is $n = 1$, and at $K = 10$, $n = 0$. Additionally, at all values of $K$, the thermal-shear mode is dominant at $Pr = 0.01$, and the thermal-buoyant mode dominates at $Pr = 10$. Therefore, the effects of Prandtl number at fixed values of $K = 0.6$ and 10 presented on Fig. 4, and the effects of $K$ at fixed values of $Pr = 0.01$ and 10 shown in Fig. 5 provide a map of the linear-instability behavior for both axisymmetric and nonaxisymmetric thermal-shear and thermal-buoyant instabilities for this flow. In addition, the weakly nonlinear results have shown that these instabilities are all supercritical.

Figure 6 illustrates the effect of $Pr$ on $\alpha$ and $c_r$ for $K = 0.6$ and 10. With the thermal-shear instability the

Table 1. Landau constants at the neutral curves for thermal-shear and thermal-buoyant instabilities. TS denotes the thermal-shear mode while TB denotes the thermal-buoyant mode

| $Pr$ | $K$ | $Gr_c$ | Type | $\alpha_c$ | $n$ | $c_r$ | $a_1$ |
|---|---|---|---|---|---|---|---|
| 0.01 | 0.6 | 13900 | TS | 2.5 | 1 | $0.19\times10^{-2}$ | $-1388+1851i$ |
| 0.01 | 10 | 15140 | TS | 2.73 | 0 | $0.42\times10^{-3}$ | $-1688+602i$ |
| 10 | 0.6 | 1522 | TB | 0.43 | 1 | $-0.38\times10^{-2}$ | $-46.9-14.3i$ |
| 10 | 10 | 5526 | TB | 1.58 | 0 | $0.43\times10^{-2}$ | $-6821+12580i$ |

variation of $\alpha$ with $Pr$ is small for both geometries. With the thermal-buoyant instability at $K = 0.6$, $\alpha$ also does not change significantly with $Pr$. In this case, however, the value of $\alpha$ is much smaller than that which occurs with the thermal-shear instability, and the disturbances associated with the thermal-buoyant mode will consist of waves that are approximately 5.5 times longer than those associated with the thermal-shear mode. In contrast to the results at $K = 0.6$, at $K = 10$, $\alpha$ increases substantially with increasing $Pr$ for the thermal-buoyant mode. In this geometry as well, however, the length of the waves associated with the thermal-buoyant disturbance are longer than those associated with the thermal-shear disturbance. For example, at a value of $Pr = 7$, which is the point at which the thermal-buoyant mode becomes dominant with increasing $Pr$, the length of the thermal-buoyant wave will be 2.8 times that of the thermal-shear wave.

The plots of $c_r$ vs $Pr$, also given in Fig. 6, show that the value of $c_r$ is nearly constant for the thermal-shear instability for both geometries. Comparison of the results with the basic-state velocity profiles shown in Fig. 2 reveals that in both geometries there are two critical layers, since the value of $c_r$ is less than the maximum base flow velocity. With the thermal-buoyant instability, at $K = 0.6$, the wavespeed is negative, and the instability will appear as a disturbance moving down the annulus rather than up as in the other cases. As will be clarified in the discussion of Fig. 7, this is a general behavior of the nonaxisymmetric thermal-buoyant instability for this problem. In the case of $K = 10$, however, $c_r$ is positive for this mode. The variation of $c_r$ with $Pr$ is also small in both geometries with the thermal-buoyant instability, but, in contrast to the thermal-shear instability, the wavespeeds are greater than the maximum (or less than the minimum) base flow velocity, and no critical layers will be present. Therefore, the wavespeeds of the thermal-buoyant disturbances will be larger than those of the thermal-shear disturbances.

As Fig. 7 illustrates, with the thermal-shear instability, $\alpha$ initially increases with increasing $K$, but

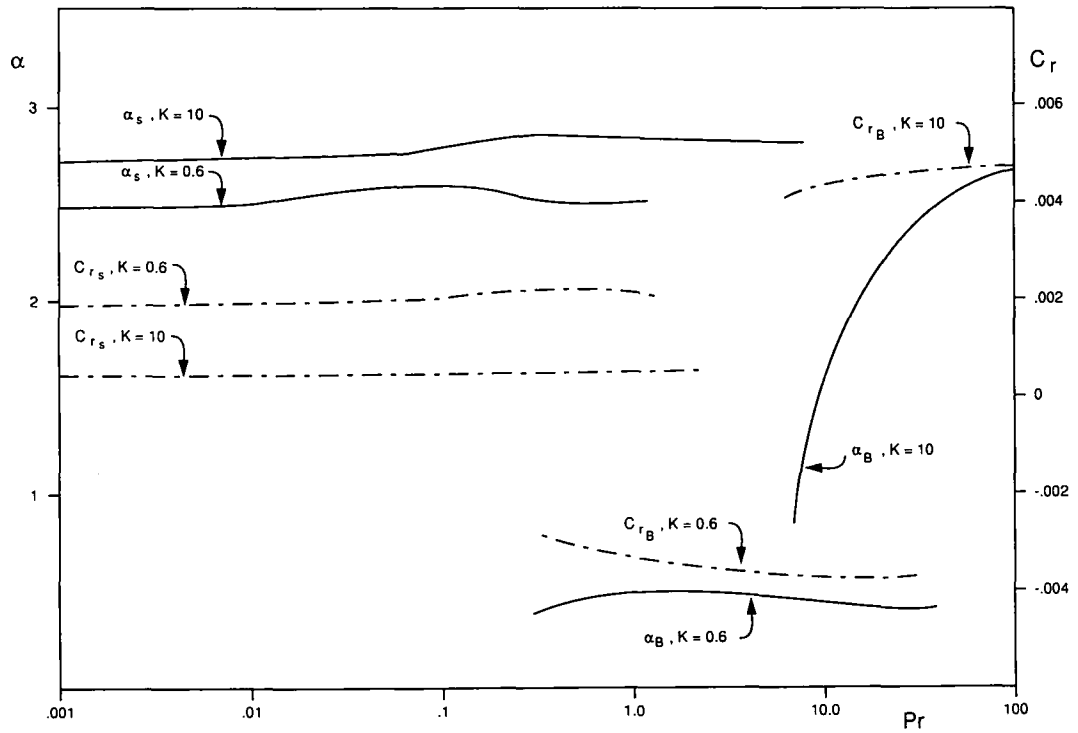


FIG. 6. Axial wavenumbers and wavespeeds vs $Pr$ for $K = 0.6$ and 10. The subscript B denotes the thermal-buoyant mode and the subscript s denotes the thermal-shear mode.

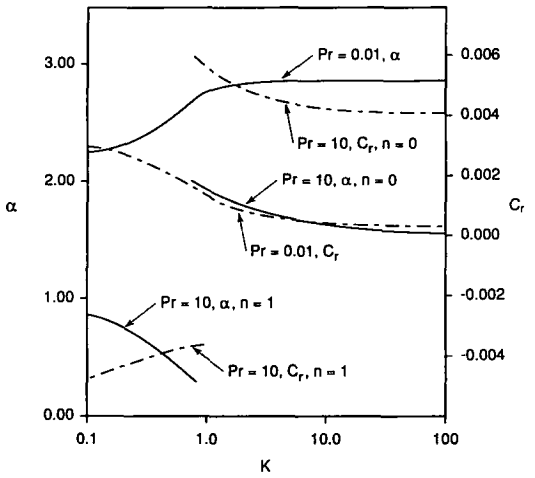


FIG. 7. Axial wavenumbers and wavespeeds vs $K$ for $Pr = 0.01$ and 10.

reaches a constant value of $\alpha = 2.8$ as a two-dimensional channel is approximated at large $K$. The plot of $\alpha$ vs $K$ for this instability is continuous, even at $K = 0.7$, where the most unstable azimuthal mode changes from $n = 1$ to 0. In contrast to the thermal-shear mode, with the thermal-buoyant instability the plot of $\alpha$ vs $K$ is discontinuous, with a jump from $\alpha = 0.35$ to 2.0 at $K = 0.9$, which is the point that the least stable azimuthal wavenumber changes from $n = 1$ to 0. Consequently, the wavelength of the non-axisymmetric thermal-buoyant disturbances at small $K$ will be much longer than the axisymmetric disturbances which occur at larger $K$.

The disturbance wavespeed for the thermal-shear disturbance, shown in Fig. 7, decreases with increasing $K$, and approaches zero at large values of $K$. Therefore, in the limit of a two-dimensional channel, the most unstable infinitesimal thermal-shear disturbance will consist of stationary waves. As with the axial wavenumber, the plot of $c_r$ vs $K$ is continuous for this instability, even near $K = 0.7$, where the most unstable azimuthal mode changes from $n = 1$ to 0. With the thermal-buoyant mode, at small $K$ the magnitude of $c_r$ decreases with increasing $K$, but still remains negative. At $K = 0.9$, however, the most unstable azimuthal disturbance changes from $n = 1$ to 0 and there is a jump in the value of the wavespeed, with $c_r$ becoming positive for $K = 0.9$ and larger. Therefore, when the first azimuthal mode of the thermal-buoyant instability is the least stable mode, the disturbance will consist of waves which travel down the channel, but when the thermal-buoyant mode is axisymmetric, the disturbances will travel up the annulus. At large $K$, in the limit of a two-dimensional channel, the thermal-buoyant instability will continue to exist as traveling waves, in contrast to the stationary waves of the thermal-shear instability.

The finite-amplitude results in Table 1, along with equation (15) show that, for the thermal-shear instability in the supercritical region ($c_i > 0$ and $(a_1)_r < 0$) the disturbance wavespeed will decrease with increasing $c_i$. However, in the limit of a two-dimensional channel at large values of $K$, the weakly nonlinear theory does not predict that the finite-amplitude disturbances will remain stationary, but rather they will drift slowly down the channel as $c_i$ increases. With the thermal-buoyant mode at $K = 10$, the disturbance wavespeed will also decrease in the supercritical region as the disturbance grows. At $K = 0.6$, on the other hand, the value of $(a_1)_i$ is negative, predicting an increase in the numerical value of the wavespeed. However, in this case the wavespeed predicted by linear theory is initially negative. Therefore, this result also predicts that the magnitude of the disturbance wavespeed will decrease as $c_i$ increases.

### 3.2. *Heat transfer*

The average Nusselt number of the flow is defined as follows:

$$Nu = \frac{h(r_o - r_i)}{\kappa} = \frac{\frac{1}{2}(1+2K)\left[\frac{\partial \theta}{\partial \eta}\right]_{\eta=0}}{\int_0^1 \theta(\eta + K)\, d\eta} \tag{16}$$

where $h$ is the convective heat transfer coefficient based on the temperature difference between the heated wall and the mean fluid temperature and $\kappa$ is the fluid thermal conductivity. A plot of the basic-state Nusselt number ($Nu_B$) vs the annulus curvature parameter, $K$, is given in Fig. 8. As may be verified from equations (5b) and (16), in the large $K$ limit, $Nu_B$ reaches an asymptotic value of $Nu_B = 3$. As the curvature parameter decreases, corresponding to an increase in the annulus curvature, $Nu_B$ increases, and reaches a value of 5.8 at $K = 0.1$.

After the equilibrium amplitude of the disturbance has been obtained, the distortion of the mean-flow may be determined from equation (12). These results can be used to predict the increase in the average

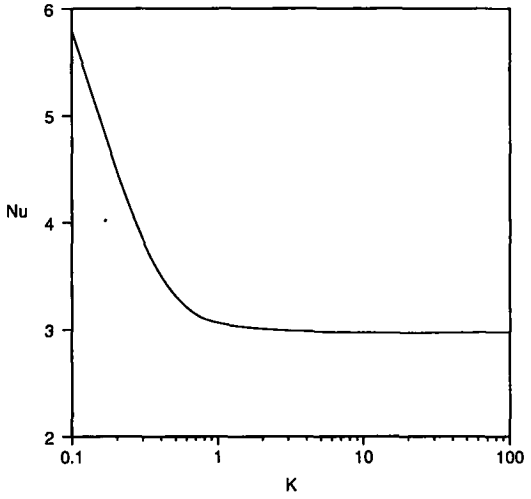


FIG. 8. Basic-state Nusselt number vs $K$.

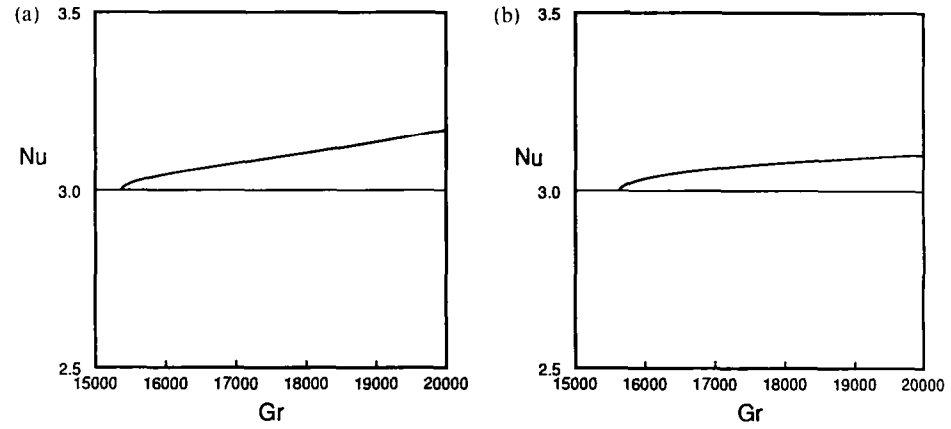


FIG. 9. Increase in $Nu$ due to flow instability for (a) thermal-shear and (b) thermal-buoyant instabilities.

Nusselt number due to the flow instability through the use of equation (16). These calculations are shown in Figs. 9(a) and (b) for both the thermal-shear and thermal-buoyant instabilities at $K = 10$. As the results show, the Nusselt numbers will increase noticeably due to flow bifurcation. The increase in $Nu$ predicted by the finite-amplitude theory is, for both instabilities, about 5%. However, as stated in ref. [10], the observed increase in heat transfer is substantially larger than this for the problem of an air gap surrounding a nuclear waste canister. Therefore, as $Gr$ increases further, the periodic flow itself will become unstable and undergo additional transitions, leading to increased transverse mixing of the fluid, and, consequently, further increases in the Nusselt number.

## 4. ENERGY TRANSFER

The kinetic energy balance of the $E^1$ wave for an axisymmetric disturbance yields the following equation

$$\frac{\partial}{\partial t}\langle \tilde{u}_1^2+\tilde{w}_1^2\rangle = -\left\langle \overline{u_1 w_1}\frac{\mathrm{d}W}{\mathrm{d}\eta}\right\rangle - \frac{1}{Gr}\langle \overline{u_1\theta_1}\rangle$$

$$-\frac{1}{Gr}\langle (\overline{\nabla u_1})^2+(\overline{\nabla w_1})^2\rangle = E_s+E_b+E_d. \quad (17)$$

The balance of thermal variance yields

$$\frac{\partial}{\partial t}\langle \tilde{\theta}_1^2\rangle = -\left\langle \overline{u_1\theta_1}\frac{\mathrm{d}\Theta}{\mathrm{d}\eta}\right\rangle - \frac{1}{Gr}\langle \overline{u_1\theta_1}\rangle$$

$$-\frac{1}{Gr\,Pr}\langle (\overline{\nabla\theta_1})^2\rangle = E_t+E_c. \quad (18)$$

In these equations, the symbols $\langle\ \rangle$ imply integration over the volume of the disturbance wave, $W$ and $\Theta$ are the mean-flow velocity and temperature distributions, respectively, and $\overline{u_1 w_1} = \tilde{u}_1 w_1 + u_1 \tilde{w}_1$, with the tilde ($\tilde{}$) denoting the complex conjugate. The terms $w_1$, $u_1$, $\theta_1$, $W$ and $\Theta$ are given by equations (11) and (12). The terms on the right-hand side of equation (17) represent an equilibrium balance of production and dissipation of disturbance kinetic energy when the disturbance amplitude has reached its equilibrium value. The first term, given the symbol $E_s$ in equation (17), represents work done by the Reynolds-stress/mean-flow strain-rate interaction, and is the shear production of kinetic energy. The second term, given the symbol $E_b$ in equation (17), represents the production of energy through work done by the fluctuating body force, and is the buoyant production of kinetic energy. The last term in equation (17), given the symbol $E_d$, represents the dissipation of disturbance kinetic energy by viscous action. In equation (18), the first term, given the symbol $E_t$, represents the gradient production of thermal variance, and the second term, $E_c$, represents the dissipation of the thermal fluctuations due to conduction.

Components of the disturbance heat flux occur in the production terms of both the disturbance kinetic energy and thermal variance. Investigation of equations (17) and (18) shows that the axial disturbance heat flux, $\overline{w_1\theta_1}$, appears in the buoyant production term in the kinetic energy balance while the radial disturbance heat flux, $\overline{u_1\theta_1}$, appears in the gradient production term for thermal variance. This illustrates that the potential energy associated with the temperature fluctuations and the kinetic energy of velocity fluctuations is exchanged through the buoyant force. However, in this problem equations (17) and (18) are not directly coupled because there are no mean gradients in the direction of the buoyant force. The energy transfer may be further clarified, however, by considering the balances for $\tilde{u}_1^2$ and $\tilde{w}_1^2$ independently as given below

$$\frac{\partial}{\partial t}\langle \tilde{u}_1^2\rangle = -\left\langle \overline{u_1\frac{\partial P_1}{\partial \eta}}\right\rangle - \frac{1}{Gr}\langle (\overline{\nabla u_1})^2\rangle \quad (19)$$

$$\frac{\partial}{\partial t}\langle \tilde{w}_1^2\rangle = -\left\langle \overline{u_1 w_1}\frac{\mathrm{d}W}{\mathrm{d}\eta}\right\rangle - \left\langle \overline{w_1\frac{\partial P_1}{\partial z}}\right\rangle$$

$$-\frac{1}{Gr}\langle \overline{w_1\theta_1}\rangle - \frac{1}{Gr}\langle (\overline{\nabla w_1})^2\rangle. \quad (20)$$

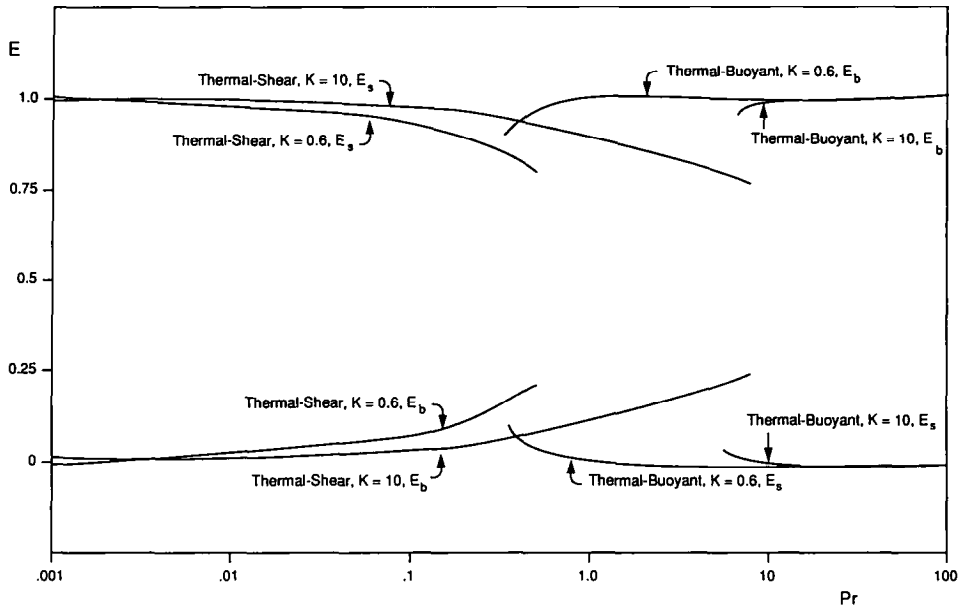


FIG. 10. $E_s$ and $E_b$ vs $Pr$ for thermal-shear and thermal-buoyant instabilities at $K = 0.6$ and 10.

Equations (19) and (20) produce the kinetic energy balance given by equation (17) when they are added since the pressure terms will be equal and opposite. However, these pressure terms account for kinetic energy that is transferred between the axial and radial components, and are called pressure scrambling terms. Equations (19) and (20) illustrate that the velocity fluctuations are initiated in the axial direction by both shear and buoyant production, while the radial velocity fluctuations are produced solely through pressure scrambling. Therefore, this term is positive in equation (19) and negative in equation (20), and a portion of the axial kinetic energy is transmitted to the radial component. Since the radial velocity fluctuations appear in the gradient production term for thermal variance in equation (18), they enhance the production of the temperature fluctuations. The temperature fluctuations in turn increase the production of axial kinetic energy through the buoyant production term in equation (17).

The integrals in equation (17) have been evaluated using the results obtained by the earlier analysis, and the results are plotted vs $Pr$ and $K$ in Figs. 10 and 11. Finite-amplitude calculations have shown that the growth of the disturbance does not significantly alter the relative amounts of kinetic energy contained in each term. Therefore, the results in Figs. 10 and 11 are those at the neutral curve, and are representative

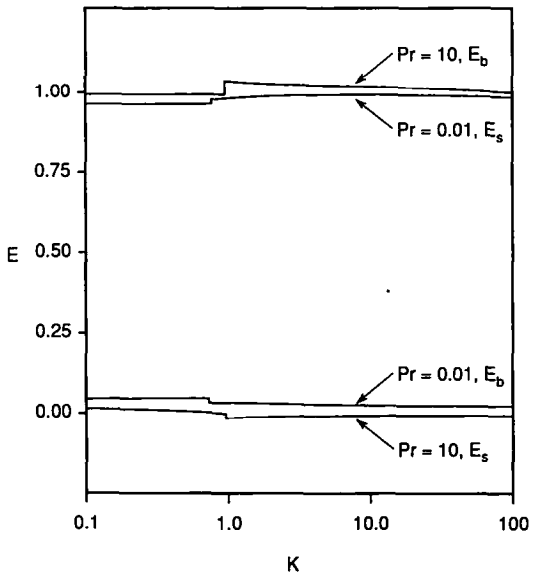


FIG. 11. $E_s$ and $E_b$ vs $K$ for thermal-shear ($Pr = 0.01$) and thermal-buoyant ($Pr = 10$) instabilities.

of the finite-amplitude disturbances as well. Investigation of Fig. 10 reveals that, with the thermal-shear instability, as $Pr$ increases, the amount of energy produced by the buoyant mechanism also increases, but the shear mechanism remains dominant. The results also illustrate that the buoyant mechanism always dominates the production of disturbance kinetic energy for the thermal-buoyant instability, but as $Pr$ decreases, shear production becomes more significant.

## 5. CONCLUSIONS

The analysis of natural convection in a tall vertical annulus with the inner cylinder heated and the outer cylinder insulated has shown that two types of supercritical instabilities exist in this flow. The parameter that determines which will be dominant in a particular geometry is the Prandtl number. The analysis of the energy transfer patterns of these instabilities has demonstrated that the low $Pr$ instability is driven primarily by shear production, and is the thermal-shear instability. The high $Pr$ instability is driven primarily by buoyant production, and is the thermal-buoyant instability. The critical value of the Grashof number does not depend strongly on $Pr$ for the thermal-shear instability, but with the thermal-buoyant mode, $Gr_c$ decreases with increasing $Pr$. In the intermediate $Pr$ range, the thermal-shear and thermal-buoyant instabilities are identified by characteristic wavenumbers and wavespeeds, with the thermal-buoyant disturbances consisting of longer, faster waves than those of the thermal-shear mode. However, with both instabilities, the first azimuthal mode is the least stable mode when the curvature of the annulus is large, and the disturbances become axisymmetric as the curvature decreases. Therefore, when the curvature of the annulus is large, corresponding to small values of $K$, the secondary flow will consist of two counter-rotating spirals, as opposed to the single traveling wave which occurs when the curvature is small.

*Acknowledgement*—Funding for this work is provided by the National Science Foundation under Grant CTS 89-13537.

## REFERENCES

1. G. K. Batchelor, Heat transfer by free convection across a closed cavity between vertical boundaries at different temperatures, *Q. Appl. Math.* **12,** 209–233 (1954).
2. E. R. G. Eckert and W. O. Carlson, Natural convection in an air layer enclosed between two vertical plates with different temperatures, *Int. J. Heat Mass Transfer* **2,** 106–120 (1961).
3. J. W. Elder, Laminar free convection in a vertical slot, *J. Fluid Mech.* **23,** 77–98 (1965).
4. J. W. Elder, Turbulent free convection in a vertical slot, *J. Fluid Mech.* **23,** 99–111 (1965).
5. L. S. Yao and B. B. Rogers, The linear-stability of mixed convection in a vertical annulus, *J. Fluid Mech.* **201,** 279–298 (1989).
6. S. A. Korpela, D. Gozum and B. B. Baxi, On the stability of the conduction regime of natural convection in a vertical slot, *Int. J. Heat Mass Transfer* **16,** 1683–1687 (1973).
7. I. G. Choi and S. A. Korpela, Stability of the conduction regime of natural convection in a tall vertical annulus, *J. Fluid Mech.* **99,** 725–738 (1980).
8. C. M. Vest and V. S. Arpaci, Stability of natural convection in a vertical slot, *J. Fluid Mech.* **36,** 1–15 (1969).
9. G. B. McFadden, S. R. Coriell, R. F. Boisvert and M. E. Glicksman, Asymmetric instabilities in buoyancy driven flow in a tall vertical annulus, *Physics Fluids* **27,** 1359–1361 (1984).
10. W. E. Lowry, B. W. Davis and H. Cheung, The effects of annular air gaps surrounding an emplaced nuclear waste canister in deep geologic storage. In *Heat Transfer in Nuclear Waste Disposal* (Edited by F. A. Kulacki and R. W. Lyczkowski), *ASME Winter Annual Meeting HTD*, Vol. 11, pp. 69–76 (1980).
11. B. B. Rogers and L. S. Yao, The effects of Prandtl number on mixed-convection in a vertical annulus, submitted for publication.
12. D. Maitra and K. Subba Raju, Combined free and forced convection laminar heat transfer in a vertical annulus, *J. Heat Transfer* **97,** 135–137 (1975).
13. L. S. Yao and B. B. Rogers, Finite-amplitude instability of nonisothermal flow in a vertical annulus, *Proc. R. Soc. Lond. A* **437,** 267–290 (1992).
14. J. T. Stuart, On the non-linear mechanics of wave disturbances in stable and unstable parallel flows—part 1. The basic behavior in plane-Poiseuille flow, *J. Fluid Mech.* **9,** 353–370 (1960).
15. J. Watson, On the non-linear mechanics of wave disturbances in stable and unstable parallel flows—part 2. The development of a solution plane-Poiseuille flow and for plane-Couette flow, *J. Fluid Mech.* **9,** 371–389 (1960).
16. K. Stewartson and J. T. Stuart, A non-linear instability theory for a wave system in plane-Poiseuille flow, *J. Fluid Mech.* **48,** 529–545 (1971).
17. W. C. Reynolds and M. C. Potter, Finite-amplitude instability of parallel shear flows, *J. Fluid Mech.* **27,** 465–492 (1967).
18. P. K. Sen and D. Venkateswarlu, On the stability of plane Poiseuille flow to finite-amplitude disturbances, considering the higher-order Landau coefficients, *J. Fluid Mech.* **133,** 179–206 (1983).
19. T. Herbert, On perturbation methods in nonlinear stability theory, *J. Fluid Mech.* **126,** 167–186 (1983).
20. A. Davey and H. P. F. Nguyen, Finite-amplitude stability of pipe flow, *J. Fluid Mech.* **45,** 701–720 (1971).